Supporting Information

Implication of Surface Oxidation of Nanoscale Molybdenum Carbide on Electrocatalytic Activity

Siying Yu, Ankit Kumar Gautam, Di Gao, Andrew N. Kuhn, Haozhen He, Alexander V. Mironenko,[*] Hong Yang[*]

Department of Chemical and Biomolecular Engineering, University of Illinois Urbana-Champaign, 600 S. Mathews Ave., Urbana, IL, 61801, USA

[*] Corresponding authors: hy66@illinois.edu (HY); alexmir@illinois.edu (AM)

Computational Notes

Note S1. Computational details

Bulk cell optimization

Bulk unit cell optimization was carried out with the bulk unit cell of β-Mo_2C (P6$_3$/mmc)[1] and optimized in VASP with the ISIF of 3 to ensure relaxation of cell dimension and angle. The electronic self-consistent field loop was executed until energy values changed by less than 10^{-6} eV and forces were less than 0.02 eV/Å.

Optimal k-point mesh in slab calculations

The optimal k-space mesh was determined using the electronic binding energy of a single oxygen atom on a clean β-Mo_2C(011) surface, defined as

$$BE_O = E_{O^*} - E_{clean} - \frac{1}{2}E_{O_2} \tag{S1}$$

where E_{O^*} is the electronic energy of the slab with a single oxygen attached to an exposed carbon atom, E_{clean} is the energy of a bare slab, and E_{O_2} is the energy of an oxygen molecule. Calculations were carried out using the PBE exchange-correlation functional. Binding energy deviations were performed for each grid against the most dense $5 \times 6 \times 1$ k-point grid, along with average CPU times per one self-consistent field (SCF) iteration (diagonalization).

Comparing the calculated values in **Table S6,** the $4 \times 5 \times 1$ grid was selected for surface calculations, because it showed errors of less than 10 meV at 2/3 of the computational cost. A more affordable $2 \times 2 \times 1$ grid was used for computationally intensive NEB and HSE06 calculations.

Dipole corrections in the z-direction

We evaluated the effect of including dipole corrections in the z-direction using the binding energy of a single oxygen atom, as described above. The inclusion of dipole corrections

only changed the energy by 3 meV (see **Table S7)**. Consequently, all surface calculations do not employ dipole corrections.

Other non-default VASP settings

We made use of ISPIN = 2 (spin polarized), ISMEAR = 0, SIGMA = 0.05 eV, IVDW = 11 for DFTD3, LREAL = Auto, and ENCUT = 450 eV. During geometry optimizations, structures were initially optimized at the Γ point, the SCF termination energy criterion of 10^{-4} eV, and until forces are less than 0.1 eV/Å. These structures served as an initial guess for calculations using a $4 \times 5 \times 1$ k-point grid, SCF loop terminating at the 10^{-6} eV energy difference, and forces less than 0.05 eV. This two-level optimization offer the opportunity for a significant speedup in obtaining optimized geometries quickly.

NEB settings

NEB calculations employed the climbing image method[2, 3] with eight images excluding the endpoints. The transition state geometry was further corrected with the dimer method using default dimer settings and EDIFF = 1e-6 eV, EDIFFG = -0.05 eV/ Å. Vibrational frequencies were computed for the transition state to verify the presence of a single imaginary mode.

Bader charge calibration

Bader charges were computed as single point calculations at the optimized geometry with the PREC = Accurate setting in the VASP input file. Software output values were then converted to net atomic charges by subtracting them from 6 (the core charge) for Mo atoms. Oxidation states of +0, +2, and +6 were ascribed to the Bader net atomic charges obtained for bulk Mo, bulk Mo_2C, and bulk MoO_3, respectively. We observed a near-linear correlation between oxidation states and Bader atomic charges and established the following relationship (**Figure S1**):

$$\text{Oxidation state} = 2.51 \times \text{BaderNetAtomicCharge} + 0.13 \qquad (S2)$$

Gibbs free energy and solvation correction

We computed the vibrational frequencies of the adsorbates (every species on the surface except slab Mo and C) and treated them using the harmonic oscillator approximation. Frequencies under 100 cm^{-1} were shifted up to 100 cm^{-1}. We approximated Gibbs free energy G as Helmholtz free energy F by neglecting the PV term, according to **Equation S3**. A temperature of 298.15 K was used in all calculations.

$$G = F = E_{elec} + E_{ZPE} + \int_0^T C_{V,vib} \, dT - TS_{harmonic} \qquad (S3)$$

We used VASPsol[4-6] to describe the solvation environment implicitly with the PBE functional and added the energy correction onto the HSE06 electronic energies:
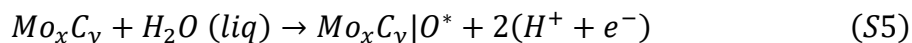
$$G_{HSE06} = E_{elec,HSE06} + (G_{PBE} - E_{PBE}) + (E_{PBE,VASPSOL} - E_{PBE}) \qquad (S4)$$
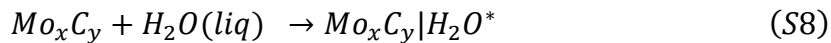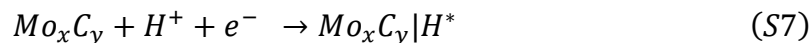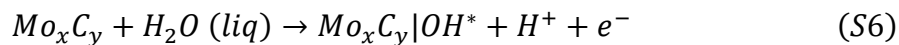
The corrections terms in **Equation S4** allow us to use solvation stabilization and the vibrational frequencies with a much faster PBE exchange-correlation functional, since both vibration and solvation effects have much less influence on relative energies than that with the electronic energy and largely cancel out in energy differences (**Table S1**).

Note S2. Gibbs free energy of formation of chemisorbed species

Binding energy of adsorbates at low coverage

We computed the adsorption energies of O*/H*/OH*/H$_2$O* on the clean surface according to **Equations S5-S8**, respectively, as shown below,

$$Mo_xC_y + H_2O \ (liq) \rightarrow Mo_xC_y|O^* + 2(H^+ + e^-) \qquad (S5)$$

$$Mo_xC_y + H_2O\ (liq) \rightarrow Mo_xC_y|OH^* + H^+ + e^- \tag{S6}$$

$$Mo_xC_y + H^+ + e^- \rightarrow Mo_xC_y|H^* \tag{S7}$$

$$Mo_xC_y + H_2O(liq) \rightarrow Mo_xC_y|H_2O^* \tag{S8}$$

In **Table S8,** we report the binding energies of chemisorbed species at the lowest possible coverage at $U_{RHE} = 0$ V for the (3×1) β-Mo₂C(011) supercell. All energies are in eV.
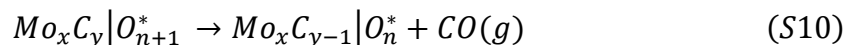
Note S3. C*-to-O* substitutiton reaction

The C* to O* substitution reaction, also referred to as substitutive oxidation, was assumed to proceed through the following steps on a partially oxidized surface containing n O* atoms:
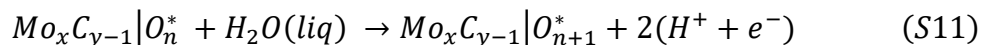
1. "Additive" oxidation of the surface

$$Mo_xC_y|O_n^* + H_2O(liq) \rightarrow Mo_xC_y|O_{n+1}^* + 2(H^+ + e^-) \tag{S9}$$
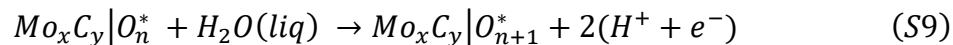
2. CO desorption to form carbon vacancy

$$Mo_xC_y|O_{n+1}^* \rightarrow Mo_xC_{y-1}|O_n^* + CO(g) \tag{S10}$$

3. "Additive" oxidation on the carbon vacancy

$$Mo_xC_{y-1}|O_n^* + H_2O(liq) \rightarrow Mo_xC_{y-1}|O_{n+1}^* + 2(H^+ + e^-) \tag{S11}$$

The net effect amounts to C* replacement with O* and the production of one CO molecule and 4 $(H^+ + e^-)$ pairs in the process. Due to the strong stabilization associated with proton-electron pair generation, substitutive oxidation is exergonic at all positive potentials (**Table S9** and **Figure S15**).

Note S4. CO and CO$_2$ desorption barriers

To evaluate the kinetics of this thermodynamically favorable substitution process, we assumed vacancy reoxidation to be fast due to the high oxophilicity of Mo. Thus, vacancy formation through CO/CO$_2$ removal is the rate-limiting step (RLS). Since CO$_2$ formation is associated with nearly complete detachment of CO* in the transition state (**Table S5**) and exhibits greater barriers than for the removal of CO (**Table 4**), we used the computed barrier for CO removal as a kinetic stability metric of oxidized surfaces. The transition state structures are obtained through CI-NEB and the dimer method. All values are in eV (**Table S5**).

Note S5. Water binding energies at oxidized surfaces

We calculated water adsorption energies on pre-determined, oxidized surfaces (**Table S4**).

Note S6. Charge transfer estimation

To obtain an order-of-magnitude estimate of the amount of charge produced in various surface oxidation processes, we employed a simplified model of a catalyst. The calculation proceeds as follows:

$$\text{Total Charge} = (\text{Charge of } 2 \ e^-)$$
$$\times \ (\text{Number of O}^* \text{added} + 2 \times \text{number of C substituted})$$
$$\times \ (\text{Estmated area of all deposited nanoparticles})$$
$$/(\text{Area of } 3 \times 1 \text{ supercell}) \qquad (S12)$$

where the charge generated from one O* deposition is 2 e$^-$.

To get the ratio of areas (*i.e.*, the number of supercells in the material), we first determined the amount of Mo$_2$C formed from the amount of a precursor, assuming total conversion of Mo to carbide during carburization:

$$\text{Moles of Mo}_2\text{C formed} = \frac{7}{2}\text{Moles of } ((NH_4)_6Mo_7O_{24} \cdot 4H_2O) \qquad (S13)$$

To determine the amount of Mo_2C on the electrode, we took into account the Mo_2C:carbon black mass ratio, the weight of a β-Mo_2C sample (3 mg), and the dilution factor during ink-drop cast of the electrode to get 9.61 μg of catalyst on a single electrode. Using 8.9 g/cm^3 density for β-Mo_2C and assuming perfectly spherical uniform 5 nm nanoparticles, we get 1.65e+13 nanoparticles on the electrode exposing a total of 1.30e-3 m^2 area. Since each computational supercell exposes 6.35e-19 m^2, we get a total 2.04e+15 unit cells. Applying **Equation S12,** we get

$$\text{Charge per O* addition} = 2 \times 1.6 \times 10^{-19} \times 2.04 \times 10^{15} \text{ mC} \qquad (S14)$$
$$\text{Charge per O* addition} = 0.65 \text{ mC}$$

Using this value, we found that the $(Mo\text{-}O)_1(C\text{-}O)_6$ to $(Mo\text{-}O)_3(C\text{-}O)_6$ change produces 1.31 mC since it involves deposition of 2 O*. On the other hand, $(Mo\text{-}O)_3(C\text{-}O)_6$ to $(Mo\text{-}O)_4(C\text{-}O)_6$ gives rise to 0.65 mC. Furthermore, achieving the surface $(Mo\text{-}O)_{12}(C\text{-}O)_0$ from $(Mo\text{-}O)_3(C\text{-}O)_6$, involves deposition of 11 O* (6 of which are removed in the CO desorption), generating a charge of 7.18 mC.

Note S7. Current estimation

We carried out a similar calculation of current densities during slow and fast substitutive oxidation using the obtained energy barrier values.

$$rate = \frac{k_B T}{h} \exp\left(\frac{-E_a}{k_B T}\right) \left[\frac{1}{\text{sec·site}}\right] \qquad (S15)$$

In this analysis, we counted the total number of exposed C sites to be 1.22e+16 and obtained the estimates of current for oxidation because of CO desorption (**Table S3**).
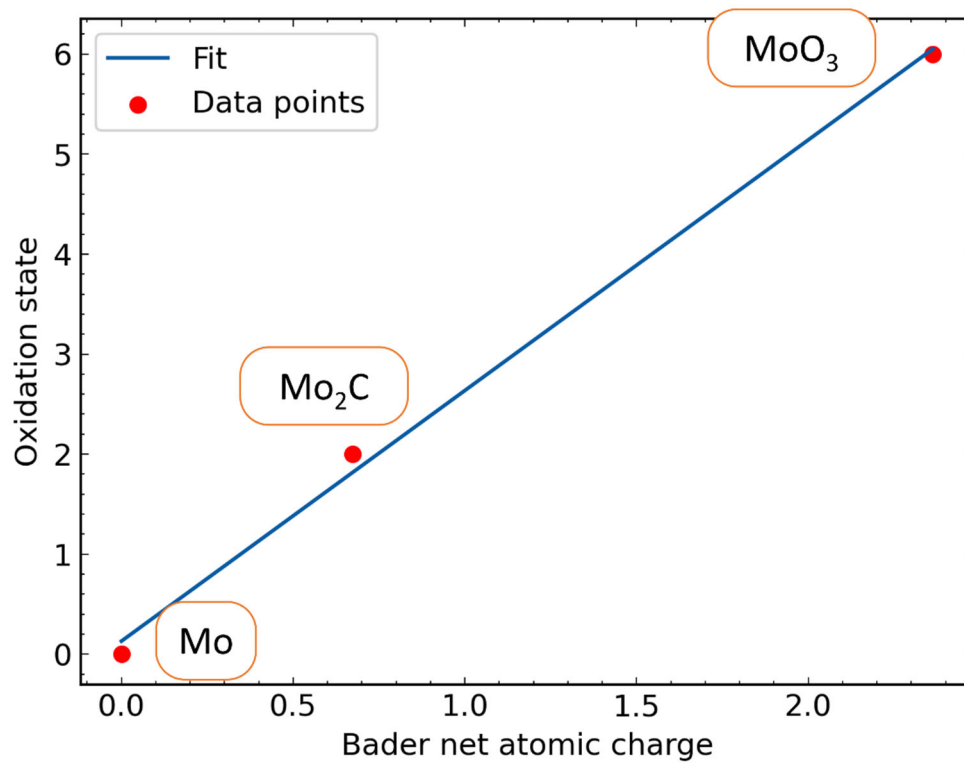
Figures

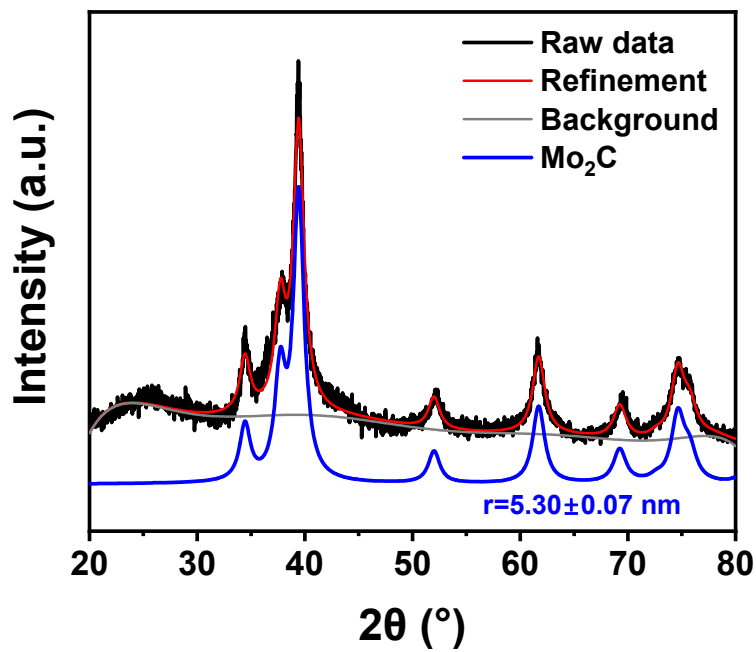**Figure S1.** Calibration curve for Bader charges and oxidation states.

Figure S2. Volume-weighted mean crystallite size (r) analysis based on the full-profile Rietveld refinement, using the TOPAS software. The calculation is based on Scherrer equation.
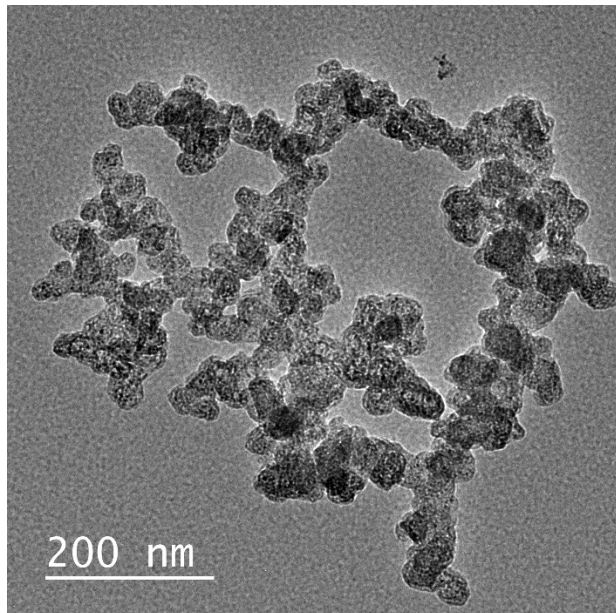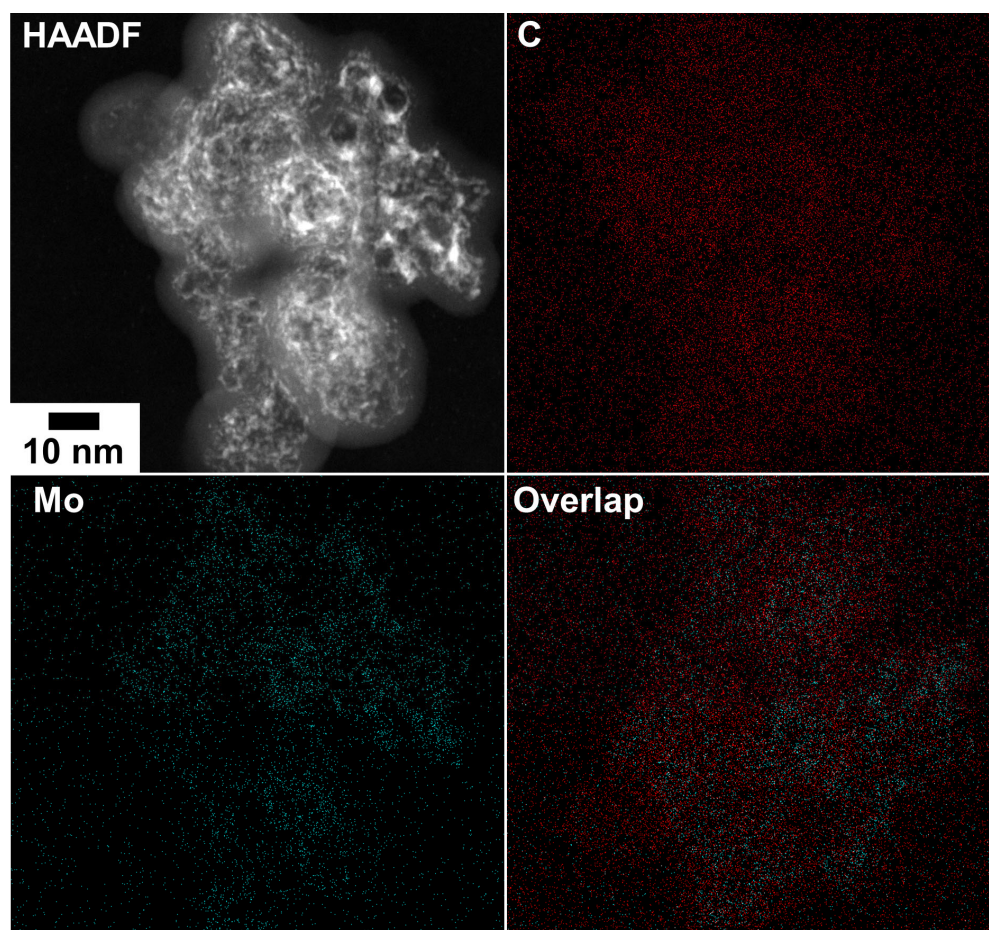
Figure S3. TEM micrograph of as-made β-Mo$_2$C sample.

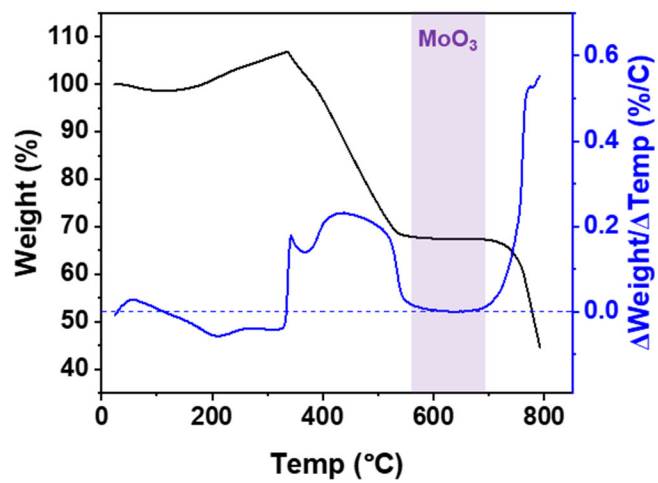**Figure S4.** STEM-EDS micrographs of as-prepared β-Mo$_2$C nanoparticles: (red: carbon; blue: Mo).

Figure S5. Thermogravimetric analysis of freshly prepared β-Mo2C sample. The purple region represents the stable MoO_3 phase.[7-9]
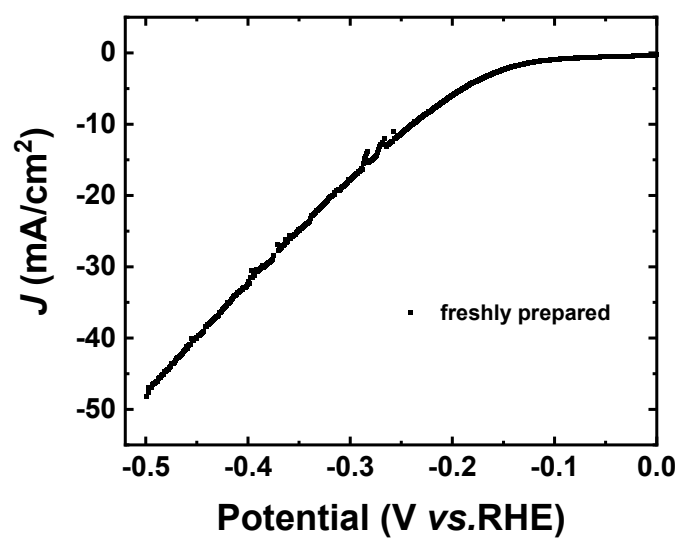
Figure S6. HER polarization curve of as-prepared β-Mo$_2$C catalyst without the electrochemical oxidation treatment.
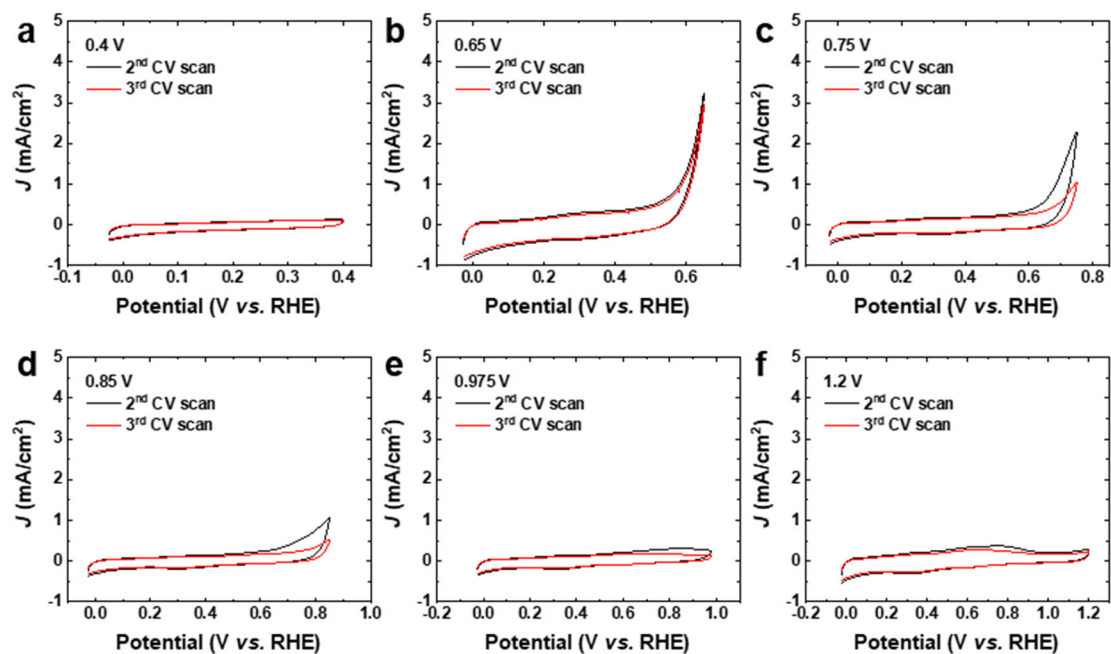
Figure S7. CV curves for the second and third cycles of the electrochemical oxidation treatment under different potential windows.
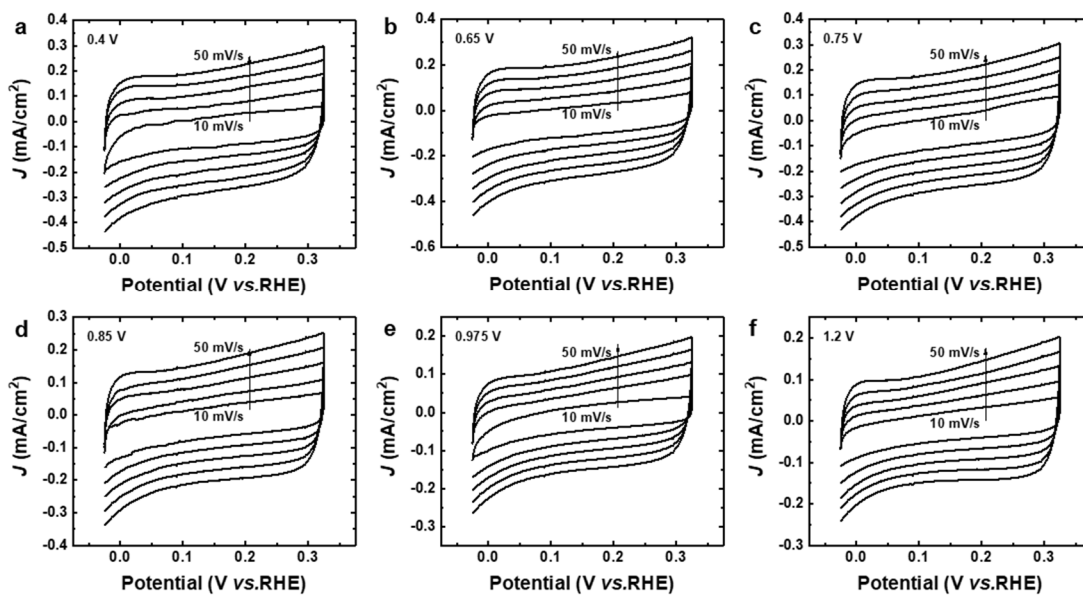
Figure S8. Measurement of double-layer capacitance. Cyclic voltammetry curves of oxidized β-Mo$_2$C-*x* catalysts scanned from 10 to 50 mV/s, where *x* is (a) 0.4, (b) 0.65, (c) 0.75, (d) 0.85, (e) 0.975, and (f) 1.2.
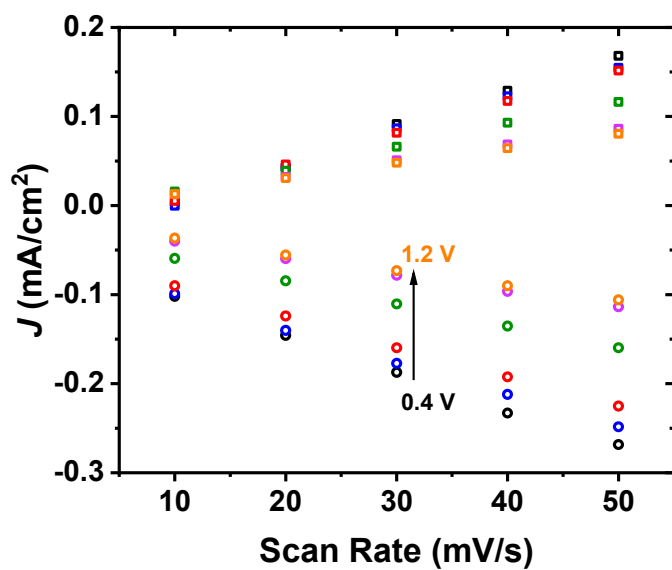
Figure S9. Capacitive current densities recorded at 0.15 V as a function of scan rate for electrochemically oxidized β-Mo$_2$C-x catalysts (square: positive scans, circle: negative scans).
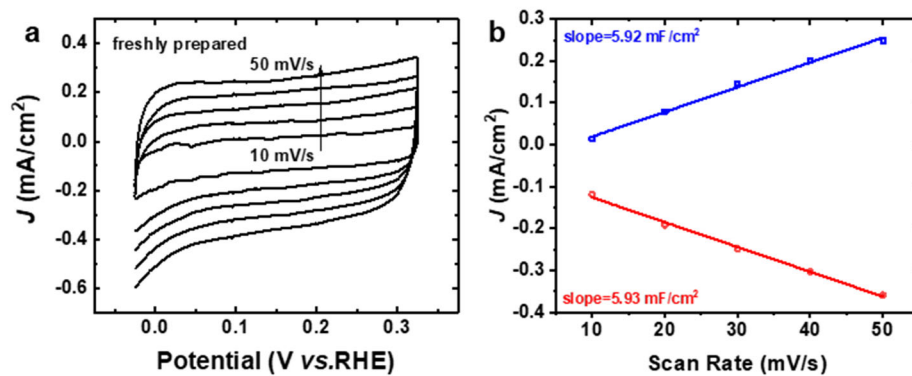
Figure S10. (a) CV curves and (b) capacitive current densities as a function of scan rate of as-prepared β-Mo₂C catalysts. The CV scans were at various rates between 10 and 50 mV/s with an increment of 10 mV/s. The capacitive current densities were measured at 0.15 V.

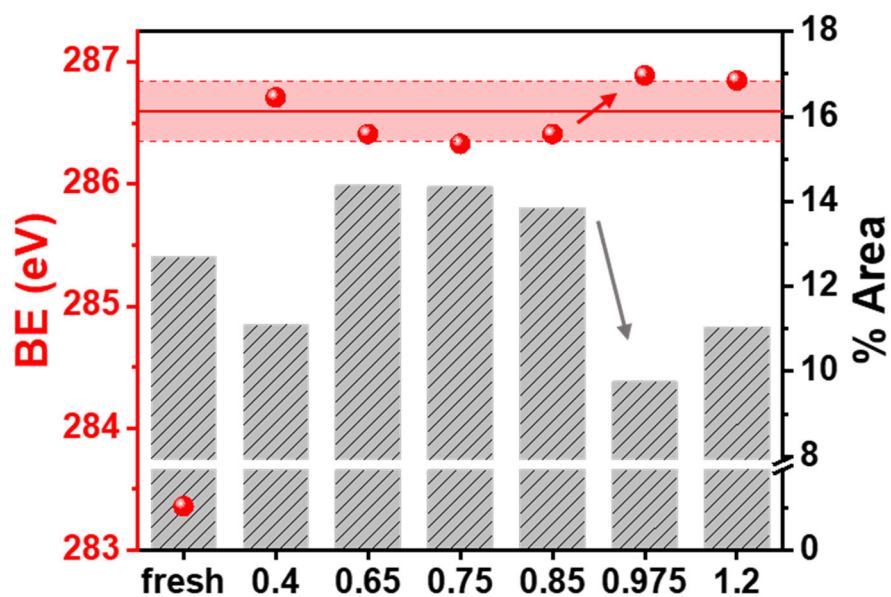**Figure S11.** XPS analysis showing the position of the broad peaks centered around 286.6 eV in the C 1s region of β-Mo_2C-x (left axis) and the corresponding percentage of peak area (right axis). The pink strip represents the averaged peak positions, in 1σ standard deviation, for β-Mo_2C-x (x=0.4, 0.65, 0.75, 0.85, 0.975, and 1.2). The carbidic C-Mo peak for freshly prepared Mo_2C is included as the reference.
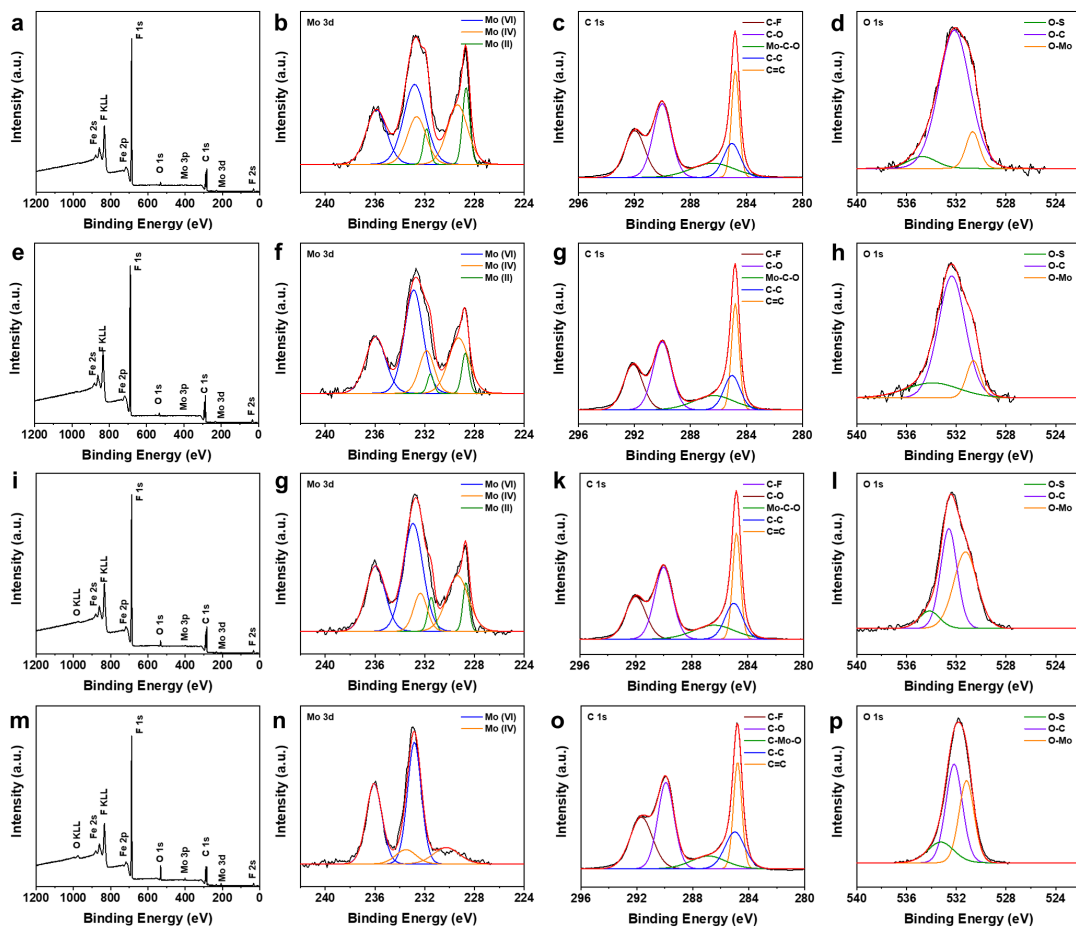
Figure S12. XPS of survey scan, Mo 3d, C 1s, and O 1s for β-Mo$_2$C-x, where x is (a-d) 0.65, (e-h) 0.75, (i-l) 0.85, and (m-p) 0.975.

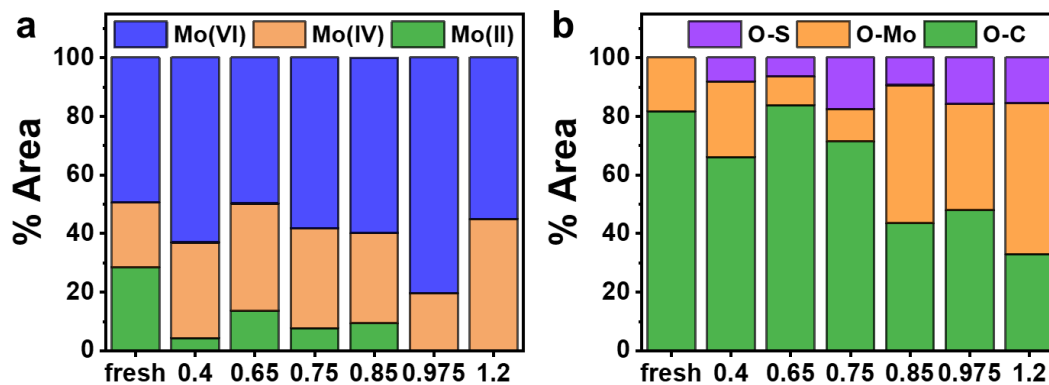**Figure S13**. Analysis of the XPS peak areas for (a) Mo and (b) O for samples treated under different potentials.
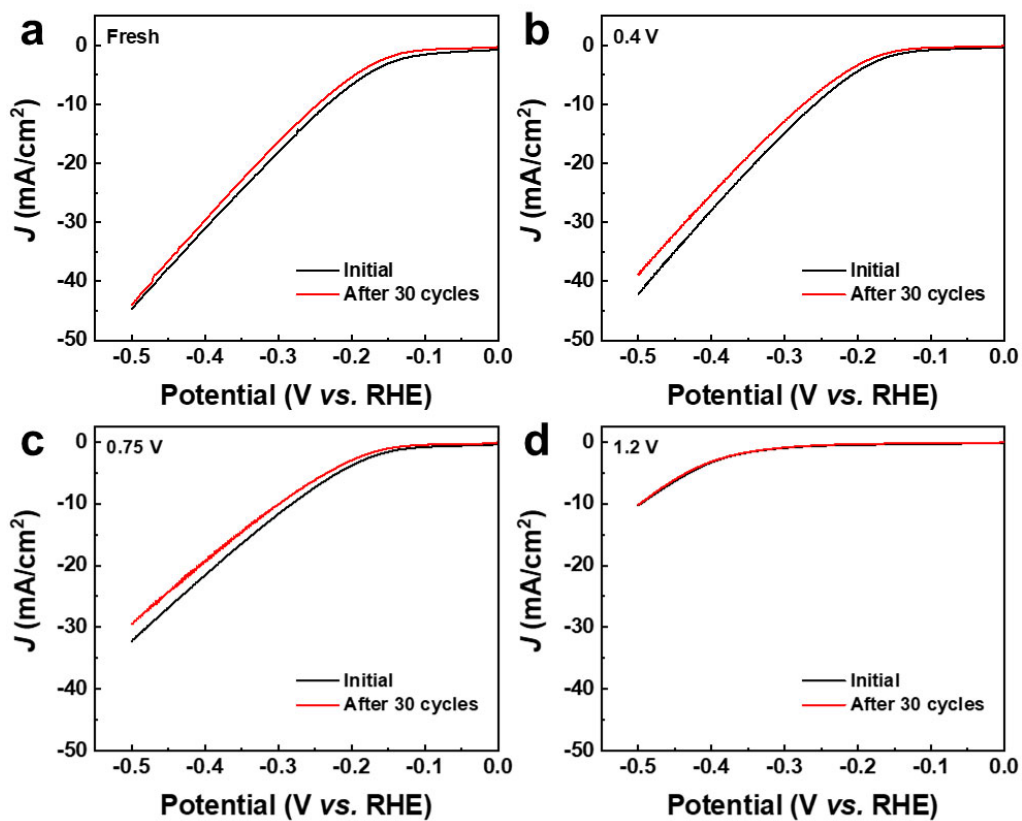
Figure S14. Polarization curves of freshly prepared and oxidized β-Mo₂C-*x* (*x*=0.4, 0.75, and 1.2) electrocatalysts for HER before and after 30 CV cycles in the range of 0~-0.5 V (*vs.* RHE).

Figure S15: Gibbs free energy for the formation of C*-to-O* substituted surfaces.

Tables

Table S1. Values of Gibbs free energy for the molecules studied in this work*

Molecule	PBE	HSE06
H_2	-6.806	-7.869
H_2O	-14.218	-17.468
CO	-15.165	-18.600
CO_2	-23.205	-28.634

*: All values are in eV.

Table S2. Results of XPS analyses

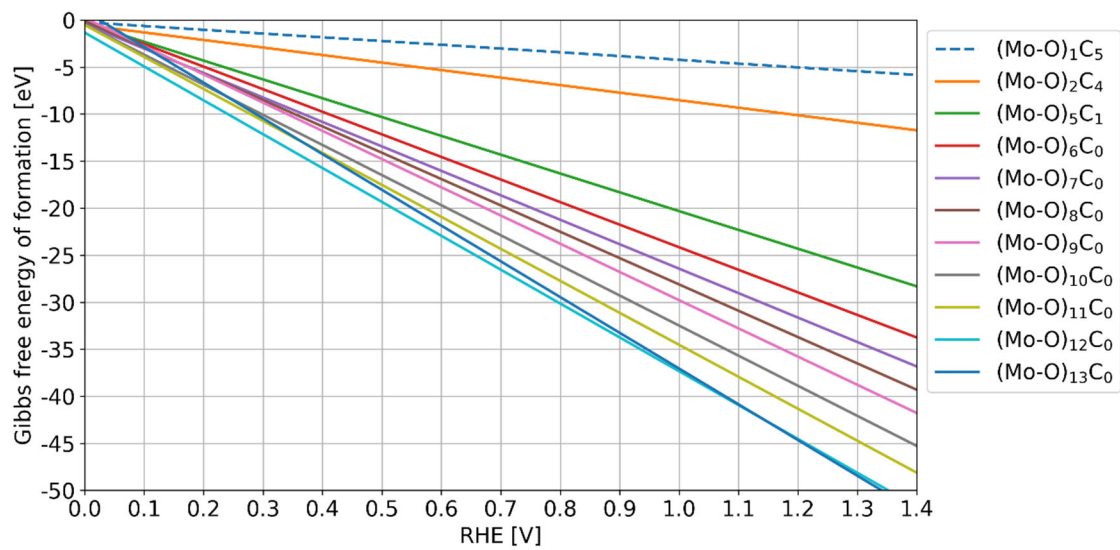|	β-Mo₂C (as-prepared)				
Name	Position (eV)	ΔBE (eV)	% Area	Area ratio	FWHM
O-C	531.98	/	81.69	/	3.07
O-Mo	530.61	/	18.31	/	1.17
C-O	286.76	/	19.91	/	5.4
C-C	284.98	/	38.79	/	1.97
C=C	284.8	/	28.6	/	0.77
C-Mo	283.36	/	12.7	/	1.27
Mo (VI) 3d$_{3/2}$	235.89	2.84	19.33	0.64198	1.97
Mo (VI) 3d$_{5/2}$	233.05	/	30.11	/	1.81
Mo (IV) 3d$_{3/2}$	232.37	2.53	8.41	0.61477	1.23
Mo (IV) 3d$_{5/2}$	229.84	/	13.68	/	1.56
Mo (II) 3d$_{3/2}$	232.7	3.91	12.49	0.7816	1.4
Mo (II) 3d$_{5/2}$	228.79	/	15.98	/	0.99
	β-Mo₂C-0.4				
Name	Position (eV)	ΔBE (eV)	% Area	Area ratio	FWHM
O-S	534.2115	/	8.15	/	1.69747
O-C	532.3142	/	66.07	/	1.82613
O-Mo	530.9864	/	25.78	/	1.71839
C-F	291.8787	/	20.65	/	1.67585
C-O	290.0209	/	30.18	/	1.58875
Mo-C-O	286.7055	/	11.11	/	2.98918
C-C	284.9736	/	17.88	/	1.53751
C=C	284.7822	/	20.18	/	0.66305
Mo (VI) 3d$_{3/2}$	235.9543	3.0678	22.73	0.5636	1.69433
Mo (VI) 3d$_{5/2}$	232.8865	/	40.33	/	1.8793
Mo (IV) 3d$_{3/2}$	232.4047	3.1317	11.51	0.54524	1.89608
Mo (II) 3d$_{3/2}$	230.813	2.0952	1.51	0.53737	0.5779
Mo (IV) 3d$_{5/2}$	229.273	/	21.11	/	1.91918

Mo (II) 3d$_{5/2}$	228.7178	/	2.81	/	0.578

β-Mo₂C-0.65

Name	Position (eV)	ΔBE (eV)	% Area	Area ratio	FWHM
O-S	534.7407	/	6.47	/	2.65846
O-C	532.1506	/	83.82	/	2.95505
O-Mo	530.6793	/	9.71	/	1.28373
C-F	291.9772	/	22.06	/	1.70079
C-O	290.0222	/	31	/	1.51986
Mo-C-O	286.4065	/	14.38	/	3.65095
C-C	285.0408	/	13.38	/	1.42234
C=C	284.8	/	19.17	/	0.64689
Mo (VI) 3d$_{3/2}$	235.89	3.0803	19.32	0.63427	1.93371
Mo (VI) 3d$_{5/2}$	232.8097	/	30.46	/	2.08344
Mo (IV) 3d$_{3/2}$	232.6444	3.2793	15.47	0.73144	1.76998
Mo (II) 3d$_{3/2}$	231.8482	3.1783	3.97	0.41225	0.60493
Mo (IV) 3d$_{5/2}$	229.3651	/	21.15	/	1.93922
Mo (II) 3d$_{5/2}$	228.6699	/	9.63	/	0.67946

β-Mo₂C-0.75

Name	Position (eV)	ΔBE (eV)	% Area	Area ratio	FWHM
O-S	533.9025	/	117.52	/	5.10628
O-C	532.3564	/	71.37	/	2.57159
O-Mo	530.619	/	11.11	/	1.30416
C-F	292.0926	/	21.21	/	1.60123
C-O	290.017	/	30.72	/	1.55048
Mo-C-O	286.3333	/	14.35	/	3.43975
C-C	285.0323	/	13.62	/	1.35511
C=C	284.8	/	20.1	/	0.64813
Mo (VI) 3d$_{3/2}$	235.9501	3.064	21.77	0.59627	1.90902
Mo (VI) 3d$_{5/2}$	232.8861	/	36.51	/	1.74481
Mo (IV) 3d$_{3/2}$	231.846	2.5652	12.3	0.56656	1.4238

Name	Position (eV)	ΔBE (eV)	% Area	Area ratio	FWHM
Mo (II) 3d$_{3/2}$	231.5364	2.8037	2.33	0.43309	0.58767
Mo (IV) 3d$_{5/2}$	229.2808	/	21.71	/	1.92779
Mo (II) 3d$_{5/2}$	228.7327	/	5.38	/	0.65256

β-Mo$_2$C-0.85

Name	Position (eV)	ΔBE (eV)	% Area	Area ratio	FWHM
O-S	534.165	/	9.4	/	1.93386
O-C	532.5974	/	43.49	/	1.56649
O-Mo	531.2625	/	47.11	/	2.21014
C-F	292.0062	/	20.48	/	1.70086
C-O	290.0153	/	30.79	/	1.51909
Mo-C-O	286.4082	/	13.85	/	3.50515
C-C	284.9947	/	14.91	/	1.47076
C=C	284.8	/	19.97	/	0.66622
Mo (VI) 3d$_{3/2}$	235.9605	3.021	22.32	0.59472	1.8292
Mo (VI) 3d$_{5/2}$	232.9395	/	37.53	/	1.86242
Mo (IV) 3d$_{3/2}$	232.351	2.9862	9.13	0.42132	1.28478
Mo (II) 3d$_{3/2}$	231.4763	2.795	4.08	0.77567	0.63659
Mo (IV) 3d$_{5/2}$	229.3648	/	21.67	/	2.08254
Mo (II) 3d$_{5/2}$	228.6813	/	5.26	/	0.57298

β-Mo$_2$C-0.975

Name	Position (eV)	ΔBE (eV)	% Area	Area ratio	FWHM
O-S	533.248	/	15.82	/	2.48381
O-C	532.1743	/	47.89	/	1.57908
O-Mo	531.1761	/	36.29	/	1.43687
C-F	291.6847	/	25.02	/	1.89404
C-O	289.9226	/	30.49	/	1.38207
Mo-C-O	286.8932	/	9.76	/	2.98105
C-C	284.9986	/	15.57	/	1.65449
C=C	284.8	/	19.16	/	0.70041
Mo (VI) 3d$_{3/2}$	236.0738	3.2426	34.47	0.75065	1.48774

Name	Position (eV)	ΔBE (eV)	% Area	Area ratio	FWHM
Mo (IV) 3d$_{3/2}$	233.5117	3.2462	7.97	0.68471	1.92654
Mo (VI) 3d$_{5/2}$	232.8312	/	45.92	/	1.30572
Mo (IV) 3d$_{5/2}$	230.2655	/	11.64	/	2.4563

β-Mo$_2$C-1.2

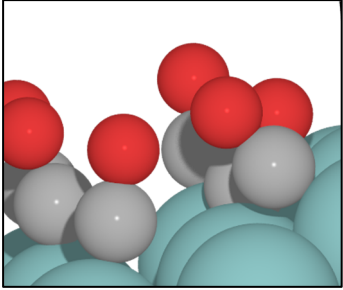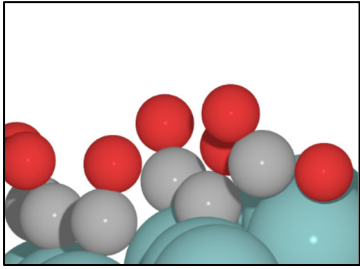| Name	Position (eV)	ΔBE (eV)	% Area	Area ratio	FWHM
O-S	533.0158	/	15.56	/	3.42747
O-C	532.1774	/	32.97	/	1.99856
O-Mo	531.5116	/	51.48	/	1.83032
C-F	291.5644	/	24.37	/	2.00869
C-O	289.9701	/	27.67	/	1.35202
Mo-C-O	286.8508	/	11.05	/	3.13211
C-C	284.9174	/	18.29	/	1.60281
C=C	284.8	/	18.62	/	0.72021
Mo (VI) 3d$_{3/2}$	236.0539	3.1551	21.69	0.64999	1.22954
Mo (IV) 3d$_{3/2}$	233.2753	4.4541	18.62	0.70745	6.67
Mo (VI) 3d$_{5/2}$	232.8988	/	33.37	/	1.20159
Mo (IV) 3d$_{5/2}$	228.8212	/	26.32	/	6.67388
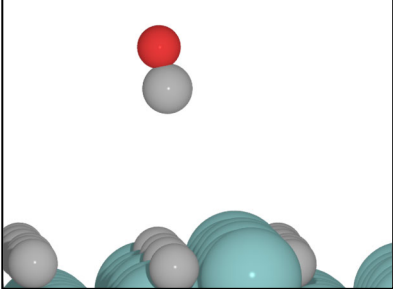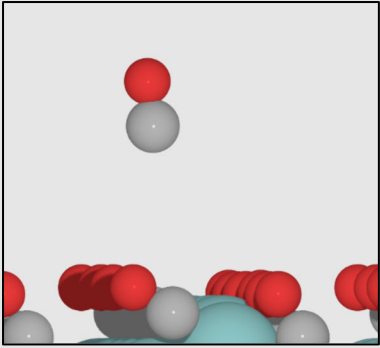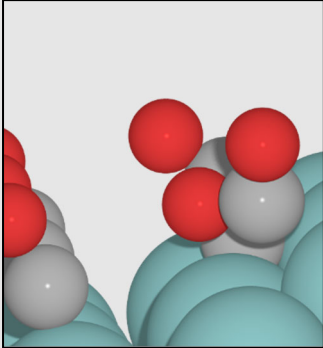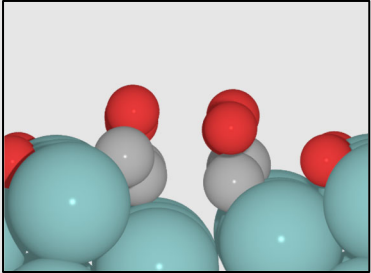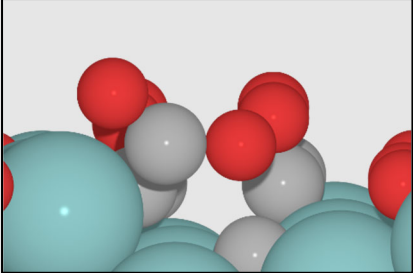
**Table S3.** Computationally obtained parameters

Potential (V)	Barrier for CO desorption (eV)	Current density (mA/cm^2)
0.28	0.71	1.24e+2
0.51	0.07	8.15e+12

Table S4. Computational results of water adsorption energy on oxidized surfaces of Mo_2C

Starting Surface	ΔG Binding energy (eV)
$(Mo-O)_0(C-O)_0$	-1.06
$(Mo-O)_0(C-O)_6$	-0.30
$(Mo-O)_1(C-O)_6$	-0.13
$(Mo-O)_2(C-O)_6$	-0.1
$(Mo-O)_3(C-O)_6$	0.19

Table S5. Energy barriers for CO and CO_2 desorptions with transition states at HSE refined single point energies. Numbers in parentheses are barriers in eV obtained using PBE functional

Surface	CO	CO_2
$(Mo-O)_0(C-O)_1$	1.39 (1.72) No TS found	-
$(Mo-O)_0(C-O)_6$	1.79 (1.98) No TS found	2.58 (2.44)
$(Mo-O)_1(C-O)_6$	1.61 (1.18)	2.75 (2.34)
$(Mo-O)_3(C-O)_6$	Type 1: 0.73 (0.84)	1.05 (1.11)

	Type 2: 0.71 (0.83)	1.37 (1.53)
$(Mo-O)_4(C-O)_6$	0 (0.07)	0.07 (0.07)
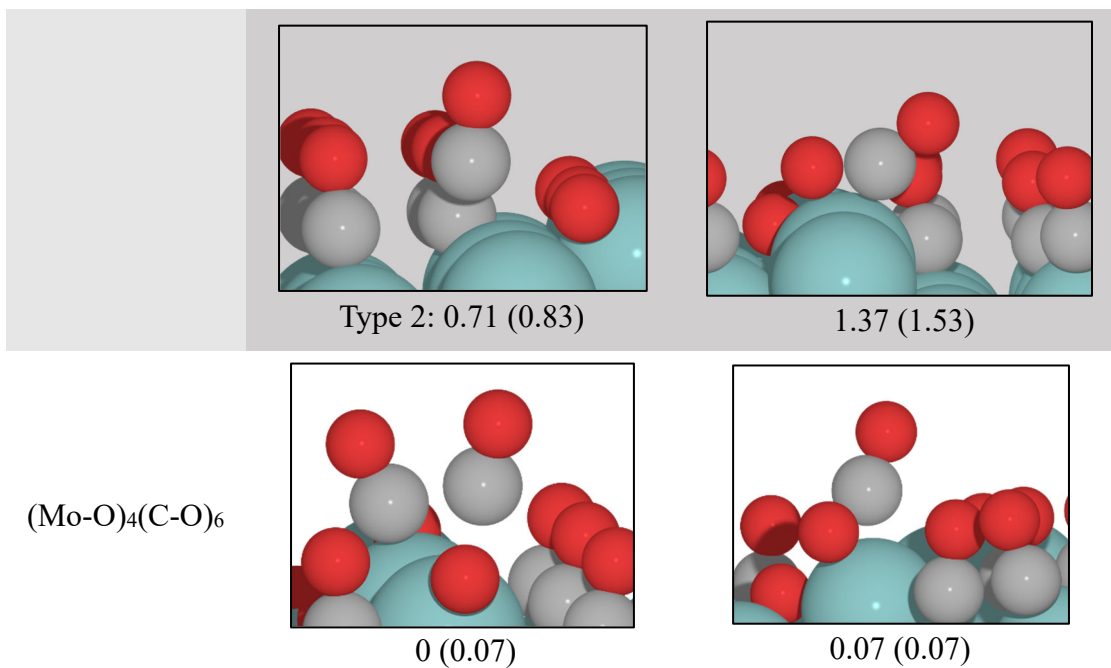
Cyan, Grey and Red balls represent Mo, C and O atoms respectively.

We also simulated CO desorption on a surface formed after substitution of three CO* molecules with three O* atoms, for which the PBE barrier was found to be 0.59 (0.47) eV.

Table S6. Convergence criteria for k point grid for surface calculations

k-point grid	ΔBE_O (eV) (against 5×6×1)	Time for 1 iteration within SCF loop (s)
1×1×1	0.485	0.34
2×2×1	-0.029	0.37
3×3×1	-0.017	1.23
4×5×1	0.007	1.86
5×6×1	0	2.76

Table S7. Influence of dipole corrections on oxygen binding energy*

	E_{clean}	E_{O^*}	$\frac{1}{2}E_{O_2}$	BE_O
No dipole	-405.546	-413.846	-4.924	-3.375
With dipole correction	-405.541	-413.843	-4.924	-3.378

*: All values are in eV.

Table S8. Binding sites for individual H_2O derived species with their energies in eV
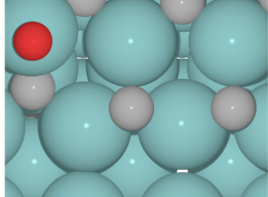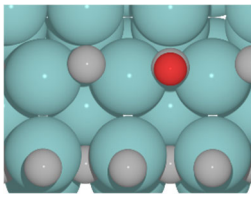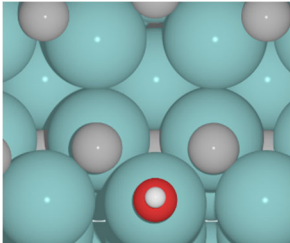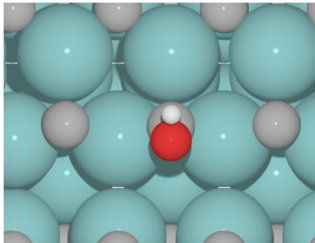
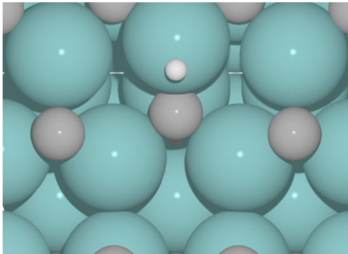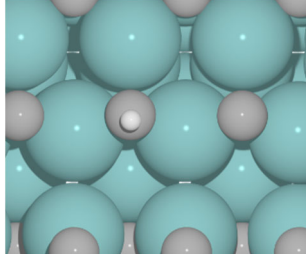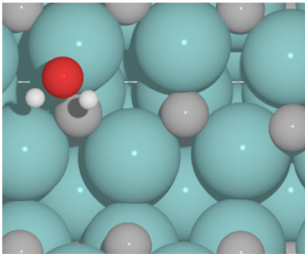| Species	Mo	C site
O*	$\Delta G = -0.26$	$\Delta G = -0.47$
OH*	$\Delta G = -0.64$	$\Delta G = -0.33$
H*	$\Delta G = -0.16$	$\Delta G = -1.12$
H_2O*	$\Delta G = -1.06$	H_2O moved to Mo or desorbs from the surface

Table S9. Gibbs free energy change for replacement of single C* to O* at two coverages

Surface prior to substitution	ΔG at $U_{RHE} = 0$ V (eV)	ΔG at $U_{RHE} = 1.2$ V (eV)
$(Mo\text{-}O)_0(C\text{-}O)_1$	-0.22	-5.02
$(Mo\text{-}O)_0(C\text{-}O)_6$	-1.02	-5.82

References

1. A. Shrestha, X. Gao, J. C. Hicks and C. Paolucci, *Chem. Mater.*, 2021, **33**, 4606-4620.
2. G. Henkelman, B. P. Uberuaga and H. Jónsson, *J. Chem. Phys.*, 2000, **113**, 9901-9904.
3. G. Henkelman and H. Jónsson, 2000, **113**, 9978-9985.
4. K. Mathew, V. Kolluru, S. Mula, S. N. Steinmann and R. G. Hennig, *J. Chem. Phys.*, 2019, **151**, 234101.
5. K. Mathew, R. Sundararaman, K. Letchworth-Weaver, T. A. Arias and R. G. Hennig, *J. Chem. Phys.*, 2014, **140**, 084106.
6. K. Mathew, Rhennig and J. Bértoli, VASPsol: VASPsol Solvation Module V1.0, https://doi.org/10.5281/zenodo.2555053.
7. R. A. Mir, P. Sharma and O. P. Pandey, *Sci. Rep.*, 2017, **7**, 3518.
8. Y. Chen, H. Zhang, J. Zhang, J. Ma, H. Ye, G. Qian, Y. Ye and S. Zhong, *Mater. Sci. Appl.*, 2011, **2**, 1313.
9. N. S. Alhajri, D. H. Anjum and K. Takanabe, *J. Mater. Chem. A*, 2014, **2**, 10548-10556.